Cite this article
Smit MS and Kearsley EP (2023)
Centrifuge modelling of ultra-thin high strength steel fibre reinforced concrete pavements.
International Journal of Physical Modelling in Geotechnics **23(1)**: 43–55,
https://doi.org/10.1680/jphmg.21.00011

Research Article
Paper 2100011
Received 13/04/2021;
Accepted 05/04/2022;
Published online 26/05/2022

International Journal of Physical Modelling in Geotechnics

ice Publishing

Centrifuge modelling of ultra-thin high strength steel fibre reinforced concrete pavements

Martha S. Smit PhD
Lecturer, Department of Civil Engineering, University of Pretoria, South Africa (Orcid:0000-0003-2882-3669) (corresponding author: phia.smit@up.ac.za)

Elsabe P. Kearsley PhD
Professor, Department of Civil Engineering, University of Pretoria, South Africa (Orcid:0000-0003-0046-3606)

Ultra-thin continuously reinforced concrete pavement (UTCRCP) is an innovative pavement type that consists of a 50 mm high strength steel fibre reinforced concrete (HS-SFRC) layer overlain on a pavement substructure. The thickness results in a flexural stiffness significantly smaller than for conventional concrete pavements. In this paper, the conceptual understanding of the response of UTCRCP to traffic loading was investigated using centrifuge modelling. Simplified pavement models were subjected to a bidirectional moving axle load. The results indicated that axle loading, and not single wheel loading, should be used to investigate the response of UTCRCP as there is significant interaction in substructure deformation caused by the wheels on the ends of an axle. Due to the flexural toughness of the highly reinforced concrete layer, a gap forms between the ultra-thin HS-SFRC overlay and its substructure. Brittle, cemented bases between the HS-SFRC overlay and subgrade should be used with caution, as the flexible nature of the layers above and below the stabilised layer may result in rapid degeneration of the brittle layer.

Keywords: centrifuge modelling/deformation/pavements & roads

Notation

E_c	concrete Young's modulus
e_{max}	maximum void ratio
e_{min}	minimum void ratio
h	concrete slab thickness
k	modulus of subgrade reaction
l_k	radius of relative stiffness
v_c	concrete Poisson's ratio
φ_{max}	maximum friction angle

1. Introduction

Ultra-thin continuously reinforced concrete pavement (UTCRCP) consists of a 50 mm thin high strength steel fibre reinforced concrete (HS-SFRC) layer placed on a pavement substructure. The HS-SFRC layer is additionally reinforced with 5.6 mm dia., 50 × 50 mm aperture steel mesh. The high reinforcement content improves the tensile mechanical behaviour, allowing for the reduction of concrete slab thickness (Barros and Figueiras, 1998; Belletti *et al.*, 2008; Briggs *et al.*, 2016; Kannemeyer *et al.*, 2007; Roesler *et al.*, 2012; Strauss *et al.*, 2007). The continuous nature of UTCRCP mitigates problems associated with expansion joints, typically used in jointed concrete pavement (JCP), and the HS-SFRC gives superior post-crack load-carrying capacity, preventing failure mechanisms such as edge-punchout, which is typically associated with continuously reinforced concrete pavements (CRCP). The reduced thickness results in a reduction in concrete material required. Although the concrete layer in UTCRCP includes high steel contents, it has been shown that the net environmental effect of high-performance concrete is smaller than its conventional counterparts due to the reduction in volume of construction materials required (Weyers, 2020).

Conventional concrete pavement types such as JCP and CRCP have thicknesses greater than 150 mm and it is due to this thickness (and flexural stiffness) that the characteristics of the material in the substructure is less important than for a road with a thin granular base and a bituminous surface seal (Brown and Selig, 1991). The ultra-thin layer of HS-SFRC in UTCRCP has a severely reduced flexural stiffness, making the properties of the substructure and its response to loading important. This paper is based on a research project where the effect of substructure stiffness on the response of UTCRCP to traffic loading was studied using scaled centrifuge models.

2. Background

2.1 Design of pavements

Pavements consist of a system of layers of unbound and bound materials, placed on top of each other and supported by the subgrade (Huang, 1993). Traffic-associated failure mechanisms of pavements are differential vertical deformation (rutting) and fatigue cracking, typically assumed to occur in the wheel path (Brown and Selig, 1991). Critical parameters are the stresses and strains used in conjunction with fatigue or rutting models

to determine the performance of pavements. The location of critical stresses and strains is unsurprisingly also typically assumed to be in the wheel path.

Broadly, there are two types of pavements, flexible and rigid pavements. Typically, concrete pavements are deemed to be rigid pavements and asphalt pavements are deemed to be flexible pavements. The concrete layer in rigid pavements forms the main structural element and can, in principle, be placed immediately over the subgrade if construction conditions allow (Brown and Selig, 1991). As the asphalt layer is not as structurally dominant as concrete, the typical design approach for flexible pavements is that the vertical stress exerted on the surface is spread gradually with depth through layers of materials that become weaker further from the surface. In terms of traffic-associated failure mechanisms, fatigue cracking is considered for rigid pavement, while rutting is ignored. Fatigue cracking, as well as rutting, are considered for flexible pavement.

Due to the high steel reinforcing content and reduced thickness of the HS-SFRC layer in UTCRCP, the concrete layer is no longer rigid or brittle and the question arises whether these pavements should be designed based on the assumptions typically made when designing rigid or flexible pavements.

2.2 Relative stiffness of pavements

The concept of relative stiffness is used to predict and describe the soil–structure interaction and, by extension, the response of civil engineering structural systems to loading. Generally, the concept attempts to take the stiffnesses of different components of a structure into account. There are two well-known relative stiffness parameters that are used in pavement design. The modular ratio uses the material stiffness of adjacent layers to enforce gradual load spreading with pavement depth. This parameter is used for the design of flexible pavements. The radius of relative stiffness is used for the analyses of slabs-on-grade, which is used for the design of rigid pavements. It is defined as a characteristic length of a pavement system and calculated using Equation 1 (Westergaard, 1926):

$$1. \quad l_k = \sqrt[4]{\frac{E_c h^3}{12(1-\nu_c^2)k}}$$

where the stiffness properties of the concrete slab are the material stiffness (Young's modulus), E_c, and Poisson's ratio, ν_c, and the thickness, h, while the stiffness of the supporting layer is quantified by the modulus of subgrade reaction, k. The modulus of subgrade reaction is determined using a plate bearing test or it can be back-calculated from the deflected shape of pavements (Bowles, 1996).

The radius of relative stiffness remains constant if E_c and k are multiplied by the same factor. The influence of the thickness of the slab on the radius of relative stiffness is raised to the power of 3. Increasing the modulus of subgrade reaction reduces the radius of relative stiffness. For the analyses of slabs-on-grade to adequately describe a two-layer system, the radius of relative stiffness should be between 570 and 2032 mm (Gerber, 2011).

2.3 Centrifuge modelling of pavements

In the recent past, a number of pavement and vehicle loading problems has been investigated using centrifuge modelling. These problems include not only pavement engineering-related problems such as the behaviour of buried pipes subjected to traffic loading (Bayton *et al.*, 2018; Saboya *et al.*, 2020), but also pavement engineering problems such as the behaviour of specific pavement types (Kearsley *et al.*, 2014; Lukiantchuki *et al.*, 2018; Smit *et al.*, 2018).

To measure the response of buried pipes to traffic loading, strain gauge arrangements on pipes were used to measure the effect of static loading (Bayton *et al.*, 2018) and rolling wheel loads (Saboya *et al.*, 2020).

To investigate the behaviour of specific pavements, the response of the pavement system to traffic loading has to be measured. Lukiantchuki *et al.* (2018) evaluated the performance of recycled construction and demolition waste (RCDW) subjected to a moving wheel. A scaling factor of 30 was used. Twenty-five bidirectional load cycles were applied. The vertical stress at the bottom of the RCDW layer was measured continuously in the centreline of the wheel path using a total stress cell, while the permanent deformation was measured indirectly as the distance the actuator had to move downward or upward to maintain the pressure of 550 kPa.

Preliminary centrifuge modelling of UTCRCP was done by Kearsley *et al.* (2014). A scaling factor of 10 was used. A shallow pavement system of four 15 mm substructure layers of different scaled granular material and a 5 mm scaled HS-SFRC layer was constructed. Bidirectional loading was applied by a moving two axle, two wheels per axle, cart. Weights were placed on the cart to maintain a pressure of 550 kPa between the wheels and the pavement surface. The pavement response was measured with linear variable differential transducers (LVDTs) that were extended and embedded in the wheel path and axle centrelines between the pavement layers. The pressure distribution underneath the concrete layer and substructure was also measured using a Tekscan™ pressure pad.

The complex model configuration and load application of Kearsley *et al.* (2014) was simplified to two- and three-layer pavement systems subjected to a moving wheel load by Smit

et al. (2018) to investigate the effect of relative stiffness on the soil–structure interaction of UTCRCP under vehicle loads. Photographs were taken at regular time intervals and discrete image correlation (DIC) was used to measure the pavement response. The radius of relative stiffness, calculated for the scaled models assuming a modulus of subgrade reaction for loose sand, was smaller than the minimum of 570 mm for the analyses of slabs-on-grade to be adequate. If a modulus of subgrade reaction for dense sand was used, the radius of relative stiffness would be smaller.

2.4 Deflection measurements

The evaluation of pavement performance includes the evaluation of distress, roughness, friction, structure, traffic, material and drainage (Huang, 1993). Deflection measurements are used to back-calculate pavement layer moduli and evaluate the structural performance of pavements. Deflection measurements are normally determined using non-intrusive measurement techniques such as the falling weight deflectometer (FWD), Benkelman beam or deflectographs (SANRAL, 2014). An FWD makes use of an impulse force, generated by dropping a predetermined weight from a predetermined height to cause deflections, which are typically measured using equally spaced velocity transducers. Deflection bowls can, however, also be determined using in situ displacement measurement of the pavement layers. For this purpose multi-depth deflectometers (MDDs) are retrofitted into pavement layers.

The techniques used in the centrifuge modelling of pavements, such as total stress cells, pressure mats and DIC, are not used in routine pavement performance evaluations and deflection bowls cannot be measured using these techniques. The measurement technique used by Kearsley *et al.* (2014) that consisted of LVDT extensions embedded between pavement layers is, however, comparable to the MDD technique and deflection bowls can be determined from the vertical displacement measurements.

The aim of this study was to use centrifuge modelling to conduct a conceptual investigation of the effect of substructure stiffness on the response of UTCRCP to traffic loading. As it was anticipated that there could be interaction between the wheels at opposite ends of an axle in UTCRCP due to the relative stiffness of the ultra-thin HS-SFRC layer and its substructure, a moving axle load was applied. The response of the pavement system (HS-SFRC layer and substructure) was monitored using the vertical displacement of the pavement layers, measured at discrete locations, similar to MDDs.

3. Experimental programme

Centrifuge modelling was conducted at the centrifuge facility of the University of Pretoria (Jacobsz *et al.*, 2014). Two simplified pavement models were tested: a two- and three-layer system. A scaling factor of 10 was used to scale the geometry of UTCRCP. The 50 mm HS-SFRC layer was scaled to 5 mm and 150 mm substructure layers were scaled to 15 mm layers. As this investigation was a conceptual study and it had been shown previously that the radius of relative stiffness of scaled UTCRCP models was smaller than the lower limit of the acceptable range for analyses of slabs-on-grade, it was not attempted to replicate a prototype radius of relative stiffness. The scaling factor was influenced by the practicality of constructing the 5 mm scaled HS-SFRC layer. A bespoke scaled model testing set-up, referred to as the centrifuge pavement tester, was developed for this study. Traffic loading was simulated using a moving two-wheel axle, subjecting the pavement model to principal stress rotation. A measurement technique similar to MDDs and the LVDT set-up used by Kearsley *et al.* (2014), referred to as mini-extensometers, was used to measure the model response. Although the centrifuge pavement tester was developed to also use DIC to monitor the pavement response, this paper will only focus on the mini-extensometer results.

3.1 Model composition

Two simplified scaled physical models of UTCRCP were tested, as illustrated in Figure 1. The first model was a two-layer pavement system with a 5 mm scaled HS-SFRC layer and 295 mm compacted dry silica sand subgrade. The second model was a three-layer pavement system with a 5 mm scaled HS-SFRC layer, 15 mm cement stabilised silica sand base layer

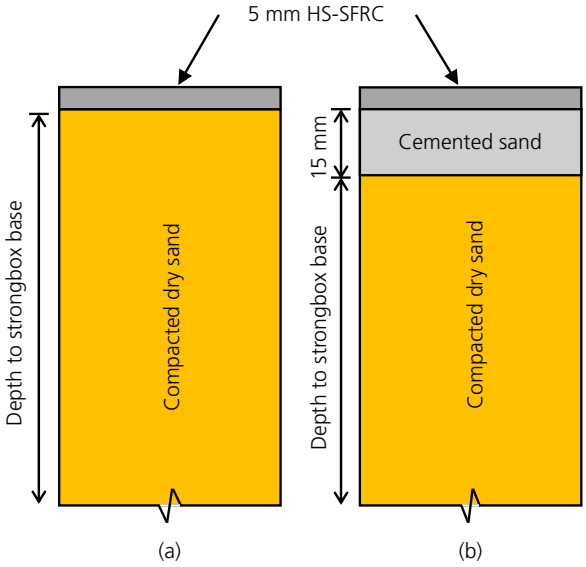

Figure 1. Simplified (a) two-layer and (b) three-layer pavement system

and 280 mm compacted dry silica sand subgrade. The total depth of both models was 300 mm.

4. Materials and model preparation

4.1 Dry silica sand substructure

Silica sand was used to construct the substructure of the centrifuge models. Figure 2 shows the particle size distribution of the silica sand. Selected properties of the silica sand were determined as shown in Table 1. The maximum and minimum density and void ratio of soil was obtained using the American Society for Testing and Materials (ASTM) standards ASTM D 4253-16 (ASTM, 2016a) and ASTM D 4254-16 (ASTM, 2016b), respectively. A maximum friction angle of the sand was determined from dry compacted and dry tested triaxial tests. Two initial confining stresses were used; 100 and 200 kPa. An average relative density of 0.82 was obtained for the triaxial samples.

The silica sand subgrade was constructed in layers using mechanical stabilisation. The upper four layers each had thicknesses of 15 mm. Dense sand was modelled for all layers, and the target relative density and dry density were 0.97 and 1617 kg/m^3, respectively. For each layer, the required mass to fill the required volume at the specified density was weighed off and compacted manually into the volume.

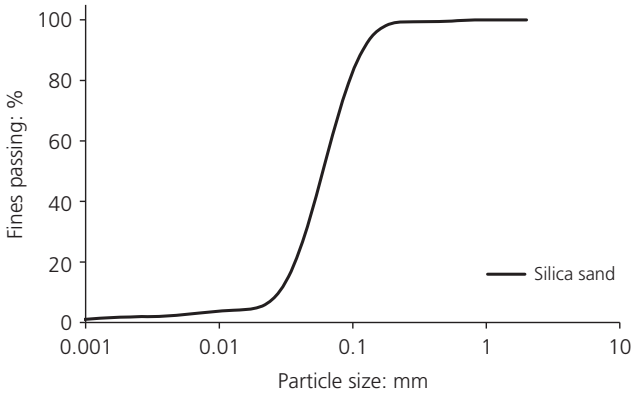

Figure 2. Particle size distribution of silica sand

Table 1. Selected properties of silica sand

Property/parameter	Value
Specific gravity	2.689
Maximum dry density: kg/m^3	1627
Minimum dry density: kg/m^3	1363
Maximum void ratio, e_{max}	0.973
Minimum void ratio, e_{min}	0.653
Maximum friction angle, φ_{max}: degrees	35.3

4.2 Cement-stabilised silica sand base

The cemented base layer was constructed using silica sand, chemically stabilised with a CEM I 42.5 R Portland cement and water. The cement content was 5% by mass and the water content was 8% water by mass. The three materials were mixed in a 10 litre drum mixer and then compacted on top of the already compacted dry sand. The target density was 1720 kg/m^3. The cemented base layer was 15 mm thick. The layer was covered and allowed to harden for 7 days before testing. The indirect tensile strength obtained using the Brazilian disc test was 120 kPa (Gaspar, 2017).

4.3 Scaled concrete overlay

The concrete mix design was adjusted from Kearsley *et al.* (2014), decreasing the maximum fine aggregate size and increasing the superplasticiser dosage. To replicate the effect of the high reinforcing content caused by the steel fibres and steel bar mesh, micro steel fibres and wire mesh were used. The fibres were 0.2 mm wide and 10 mm long. The wire mesh had a diameter of 0.5 mm and an aperture of 5 mm $\times$ 5 mm. To ensure bond between the mesh and concrete, the mesh was treated with hydrochloric acid to increase its surface roughness. The mix design and reinforcing can be seen in the paper by Smit and Kearsley (2018), along with the casting procedure and placement of the overlay on the sand substructure. As shown by Kearsley *et al.* (2014), the load–deflection behaviour of the scaled reinforced concrete layer was comparable to its full-scale counterpart.

4.4 Centrifuge pavement tester

All elements of the centrifuge pavement tester set-up are shown in Figure 3. Three of the model box sides consisted of 50 mm thick aluminium panels. The fourth side of the box consisted of a 30 mm thick glass window. The inside dimensions of the box were 600 $\times$ 460 $\times$ 300 mm.

The wheels had solid rubber tyres causing an elliptical contact area 22 mm wide and 33 mm long (depending on the load). The wheels were spaced at 220 mm centre to centre on an axle. Weights were placed on the axle to apply the desired pressure to the pavement model. The axle was attached to a sleeve that could move along a motor-driven rotating threaded shaft. The attachment to the sleeve allowed the axle to move freely in the vertical direction.

Figure 3(a) shows the location of the measurement mechanism (mini-extensometers) embedded in the strongbox base. Figure 3(b) shows the needles that extend from the mechanism into the model to measure the vertical displacement at different depths below the pavement surface in the axle and wheel path centreline. Figure 4 shows the centrifuge pavement tester after

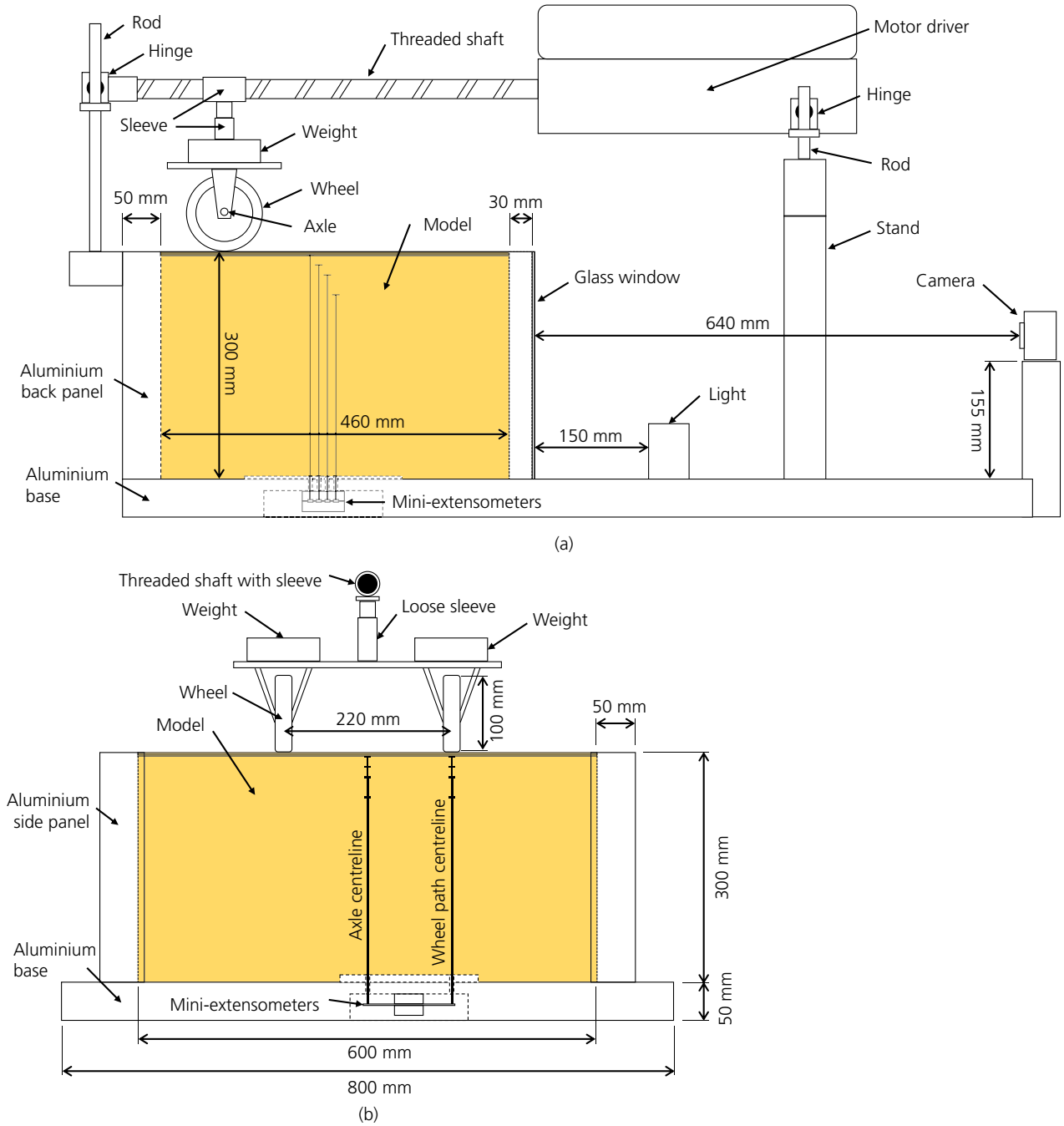

Figure 3. Schematic (a) side and (b) front section view of centrifuge pavement tester

model preparation and when placed on the centrifuge model platform.

4.5 Mini-extensometers

The mini-extensometer measurement mechanism consisted of steel bending beams that were rigidly clamped between two aluminium blocks. The bending beams were instrumented with 120 Ω strain gauges, assembled in a full Wheatstone bridge, positioned close to the clamped end of the bending beam where large bending moments would be induced when the end of the beam displaced in the vertical direction.

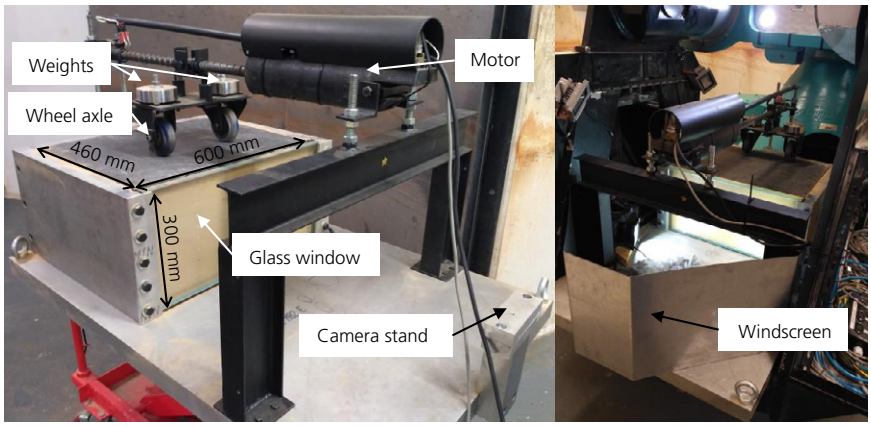

Figure 4. Centrifuge pavement tester (a) after model preparation and (b) placed in centrifuge

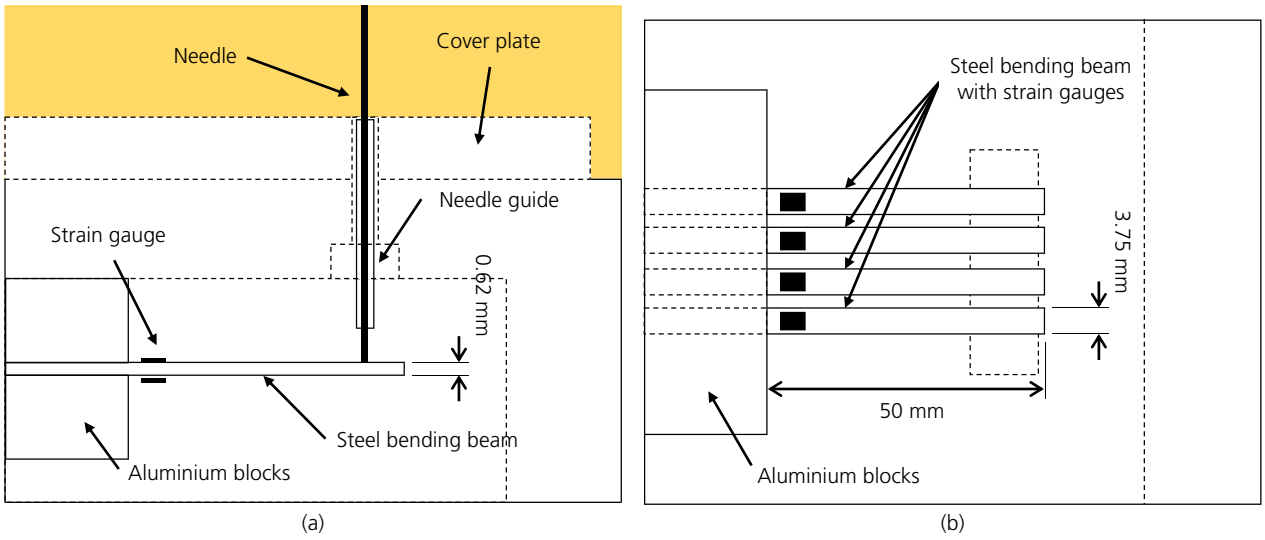

Figure 5. Measurement mechanism in (a) profile and (b) plan

A needle, embedded in the model, rested on the loose end of the bending beam causing it to deflect as vertical movement occurred in the model. Hypodermic needles were used. The embedded needles had a diameter of 0.81 mm and were flexible. To ensure that the needles rested on their respective bending beams, each needle was guided within another hypodermic needle that was fixed to the centrifuge pavement tester base. Figure 5 shows the components of the mini-extensometers.

Two sets of four bending beams were embedded in the centrifuge pavement tester base making it possible to measure movement at four depths in one of the wheel paths and along the centreline of the axle. The depth at which movement was monitored could be customised. Thin platforms were epoxied to the top end of each of the needles. This was done to ensure that the needles moved with the substructure. During model preparation, the needle-end platforms were positioned at different depths in the model. The substructure was constructed around the needles, taking care to ensure that the surrounding material was compacted to the same degree as the rest of the model.

The mini-extensometer mechanism set-up was similar to that of spring-loaded LVDTs, where the displacement that each

needle measured is the displacement of the layer above the needle, as the platform at the end of the needle pushed against the upper layer due to pre-loading of the steel bending beams.

4.6 Testing procedure

The models were constructed and placed on the model platform. The strongbox was accelerated to 10***g*** after which the loaded axle was moved over the pavement models. A pressure of 550 kPa was applied to the models through the wheels. This is representative of a standard 80 kN axle load. The pressure was not adjusted during testing. Bidirectional cycles were applied to the pavement models.

5. Results

5.1 Vertical displacement with time

Figure 6 shows the vertical displacement, measured underneath the concrete layer in the wheel path centreline (referred to as wheel centreline for the remainder of the text), caused by the first two bidirectional load cycles applied. The loaded axle moved off the glass panel onto the model and travelled towards the back panel. Due to space constraints, the axle stopped 75 mm from the back panel. It then moved back, coming to rest on the glass panel. The vertical displacement peaks occurred when the axle moved over the mini-extensometer, 230 mm away from the glass panel. There are two peaks per bidirectional cycle. These are marked as points A1 and C1 in the first cycle, and points A2 and C2 in the second cycle. Points B1 and B2 indicate where the axle stopped and changed direction. Points D1 and D2 indicate where the axle came to rest on the glass panel. This is also when the pavement model was completely unloaded and the permanent displacement could be measured. There is an accumulation of permanent displacement because the vertical displacement of the second bidirectional cycle is more than that of the first bidirectional cycle.

These results indicate that the maximum vertical displacement increased each time the wheel passed over the mini-extensometer, regardless of the direction of travel. It was thus decided that for the remainder of this paper each wheel pass would be considered as a load cycle.

Figure 7 shows the vertical displacement in the wheel centreline at depths 0, 15, 30 and 60 mm below the concrete layer, as 60 load cycles were applied. Points A1, B1, C1 and D1 are indicated as in Figure 6. The vertical displacement could be measured continuously using the mini-extensometers, making it possible to determine:

- deflection bowls in the longitudinal direction of the pavement
- vertical displacement distributions (VDDs) and
- deflection bowl change with load cycles.

Deflection bowls and VDDs will be used to discuss not only expected trends, such as decreasing rate of accumulation of permanent displacement as load cycles are applied or reduction in vertical displacement with distance from the pavement surface (Figure 7) but also trends that were unexpected.

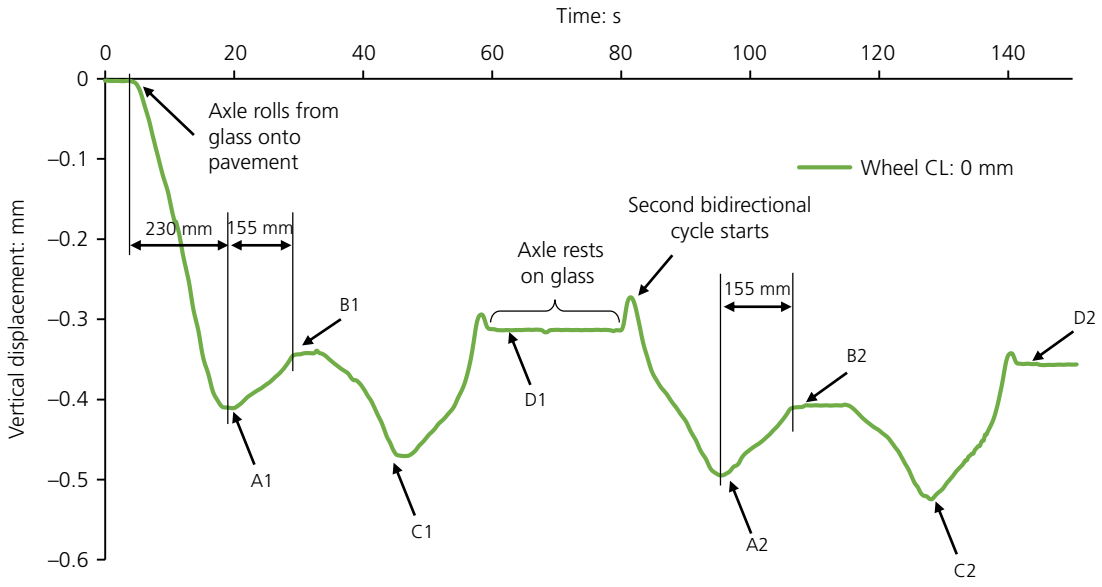

Figure 6. Vertical displacement in wheel centreline (CL) under concrete layer of two-layer pavement model

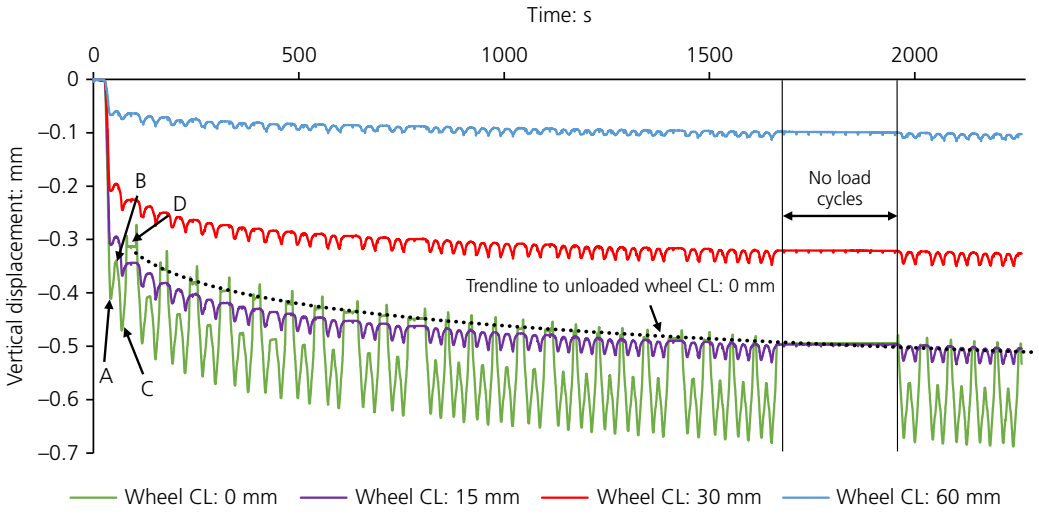

Figure 7. Vertical displacement in wheel centreline (CL) plotted against time for two-layer system

5.2 Deflection bowls of first load cycle

The deflection bowls of the first load cycle were determined from when the axle moved onto the model until it moved over the mini-extensometer for the first time – that is, the first peak measured in Figure 6. The width of the deflection bowl could not be greater than 230 mm, as that is the distance between the mini-extensometer and the glass face of the strong box. The shape of the deflection bowls was influenced by the concrete not being continuously bonded to the substructure.

Figure 8 shows the deflection bowls determined for the two- and three-layer pavement models. The deflection reduced with depth and the deflection in the axle centreline was smaller than the deflection in the wheel centreline for both models. The deflection of the model that included the cemented base was smaller than that of the model that only had a thin concrete overlay. Close to the concrete surface the deflection in the wheel path was, as expected, more than the deflection between the wheels under the axle centreline for both models.

For the two-layer pavement in Figure 8(a), at depth 30 mm, the deflection in the wheel centreline and axle centreline had a similar magnitude. At depth 60 mm the deflection in the wheel centreline was smaller than in the axle centreline. The maximum vertical displacement moved from the wheel centreline to the axle centreline at a depth between 30 and 60 mm. This observation shows that the maximum vertical strain per depth in the subgrade of UTCRCP does not necessarily occur under the load location when complex load configurations are used and that the wheel interaction may result in critical parameters at locations other than what is typically assumed. This observation would not have been made had the load configuration been a single wheel.

As seen in Figure 8(b), the deflection bowl width of the concrete layer of the three-layer model was smaller than for the two-layer model, which is due to the stiffness of the cemented sand layer being greater than the stiffness of the compacted dry sand substructure. The deflection bowl shape of the three-layer system could have been influenced more by the concrete layer not being continuously bonded to the cemented layer than the deflection bowl shape of the two-layer system. The shape of the deflection bowls could also have been influenced by the cemented base cracking during the first load cycle.

The deflection of the concrete layer was upward from an offset of 120 mm to 170 mm, indicating that tensile stresses are induced at the top of the concrete layer. The deflection bowls at depth 30 and 60 mm were shallow and narrow with no significant difference in deflection with depth in the axle centreline.

5.3 Vertical displacement distributions

Figures 9 and 10 show the loaded (L) and unloaded (UL) VDDs of the two- and three-layer models, respectively. VDDs show the vertical displacement with depth. Unloaded VDDs show the accumulation of permanent displacement with number of cycles. The figures show how the vertical displacement decreased with depth when the models were loaded and that the system steadily displaced downward as more cycles were applied.

Figure 9(a) shows that the difference between the loaded displacement at the top of the system and at the bottom of the system increases in the wheel centreline for every cycle. The

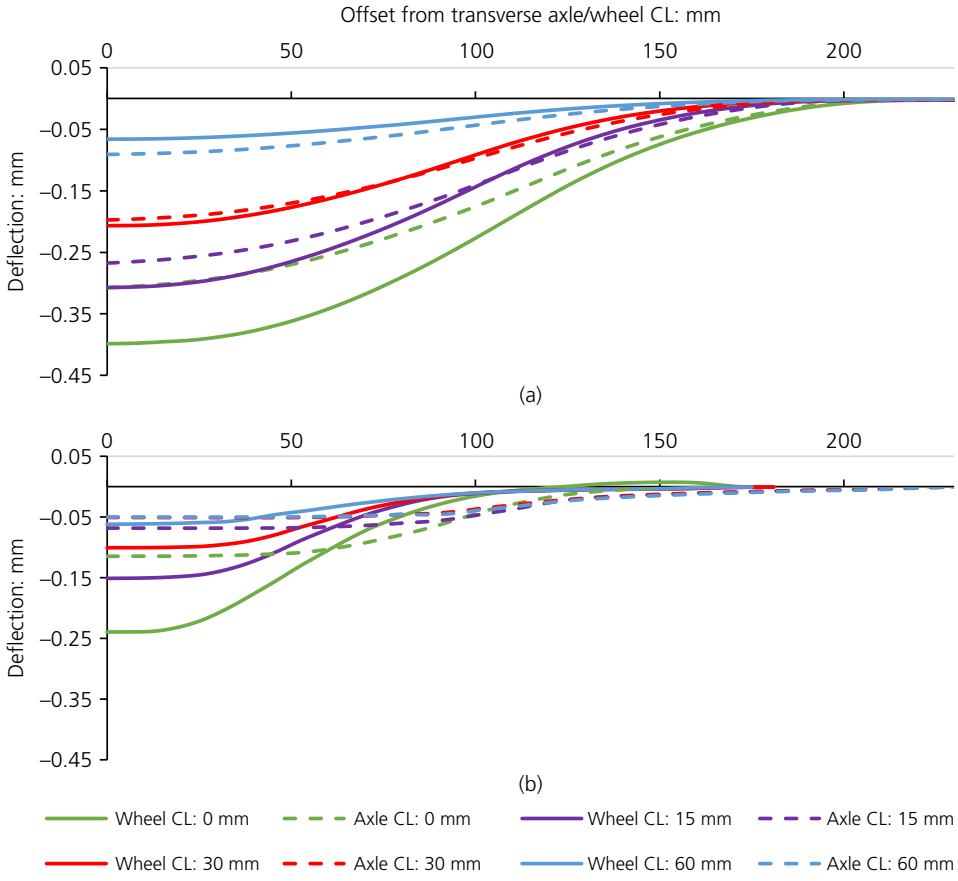

Figure 8. Wheel and axle centreline (CL) deflection bowls of (a) two-layer and (b) three-layer pavement models

shape of the loaded and unloaded VDDs of the two-layer system in the wheel centreline differed. The permanent displacement underneath the concrete layer was less than at a depth of 15 mm. The difference between the permanent displacement at 0 and 15 mm decreased as more cycles were applied. The mini-extensometer mechanism was similar to that of spring-loaded LVDTs, where each needle would measure the displacement of the layer above the platform on the end of the needle. The fact that the displacement of the concrete layer was less than what was measured in the substructure indicated that the concrete lifted off the substructure when the pavement was unloaded, indicating that a discontinuity and gap between the concrete layer and substructure had formed. The loss of support in the wheel path could also result in the location of the critical stress in the concrete layer and the supporting layers moving to a position adjacent to the wheel path.

Figure 9(b) shows that the difference in displacement at 0 mm relative to 15 mm, in the axle centreline, is smaller in comparison to displacement at the same depths in the wheel centreline. This could be attributed to overlapping zones of influence of the respective wheel loads and upward deflection (in comparison to the unloaded condition) in the axle centreline.

Figure 10(a) shows that unlike the two-layer system, the difference between the displacement at depths of 0 and 15 mm for the three-layer system increased, with more displacement occurring at 0 mm in comparison to at 15 mm. This indicates that the cemented base deteriorated as more load cycles were applied. After 40 load cycles were applied, the displacement at depths of 15, 30 and 60 mm were more stable than at 0 mm where the rate of accumulation of permanent displacement had not stabilised. The displacement in the axle centreline, as shown in Figure 10(b), was very small and stabilised after a few cycles. The possible cracking of cemented bases under ultra-thin concrete layers should be investigated using finite-element modelling to clarify this trend.

5.4 Deflection bowl change with cycles

Figure 11 shows the deflection bowl changed as more load cycles were applied for the two- and three-layer models. The

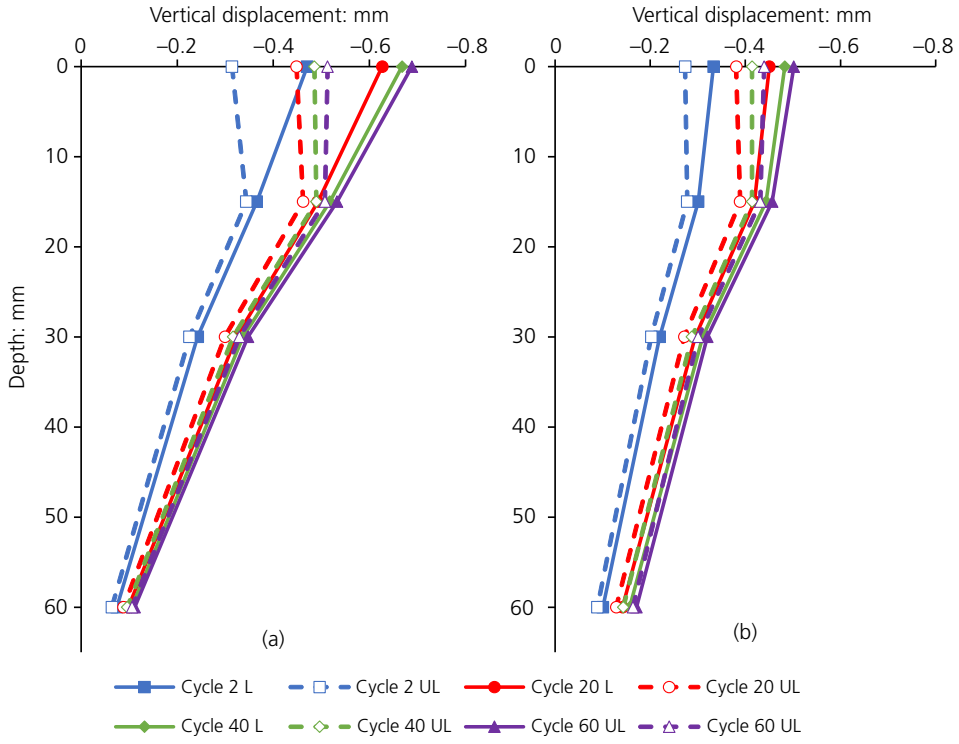

Figure 9. Loaded (L) and unloaded (UL) VDDs of two-layer system in (a) wheel centreline and (b) axle centreline

deflection bowls used in Figure 11 were determined from point A1 to point B1 for cycle 1 (see Figure 6), and from similar points on the displacement–time plot for cycles 10, 20 and 40. The model is not unloaded at point B1, but the deflection bowls are zeroed using the displacement measured at this point after the relevant cycle. The width of the deflection bowl could thus not be greater than 155 mm, as that is the distance from which the model is loaded. The displacement measured directly underneath the concrete layer was used. As seen in Figures 9 and 10, the overall displacement of the three-layer system was approximately 30% smaller than that of the two-layer system.

For the two-layer model the relative displacement at offset 0 mm, or when the load was at the measurement location, was approximately 0.065 mm for the first load application. This increased to approximately 0.10 mm for cycle 10 and did not increase significantly for cycles 20 and 40. The shape of the deflection bowls remained constant. For the three-layer model, that incorporated a cemented base layer underneath the concrete layer, the peak relative displacement after the first load was 0.05 mm and increased to 0.10 mm after ten cycles. The peak relative displacement continued to increase from cycle 10 to cycle 20 to cycle 40, albeit at a slower rate.

These results show that the two-layer system stabilised after a small number of load cycles and that the three-layer system had not stabilised after the same number of load cycles. The increasing peak relative displacement of the three-layer system deflection bowls indicates that the substructure is deteriorating. This deterioration can be caused by the crumbling of the cemented base itself or the deformation of the substructure underneath it that is subjected to stress concentrations induced by the edges of the discretely cracked cemented base.

6. Conclusions

The conceptual understanding of the response of UTCRCP to traffic loading was improved by using centrifuge modelling and measurement techniques similar to that used in industry. The mini-extensometer measurement system allowed the pavement response to be measured in terms of vertical displacement at a high frequency at different depths and transverse locations. Longitudinal deflection bowls and VDDs were determined from the vertical displacement data. The following conclusions could be drawn from the results.

- The maximum vertical strain per depth in the substructure of UTCRCP does not necessarily occur under the load

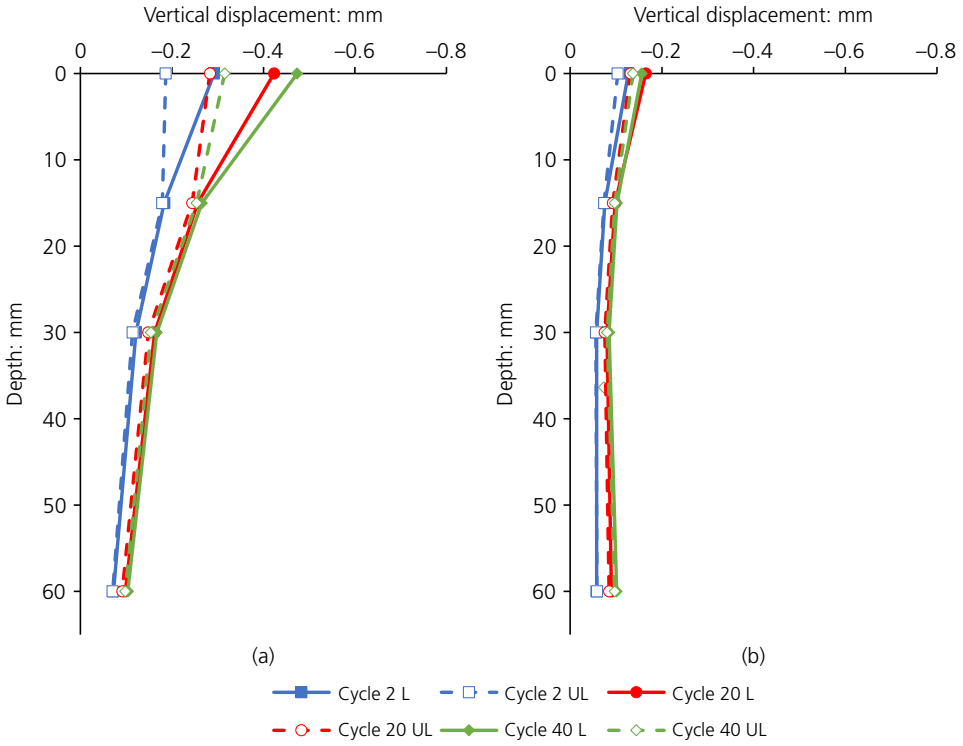

Figure 10. Loaded (L) and unloaded (UL) VDDs of three-layer system in (a) wheel centreline and (b) axle centreline

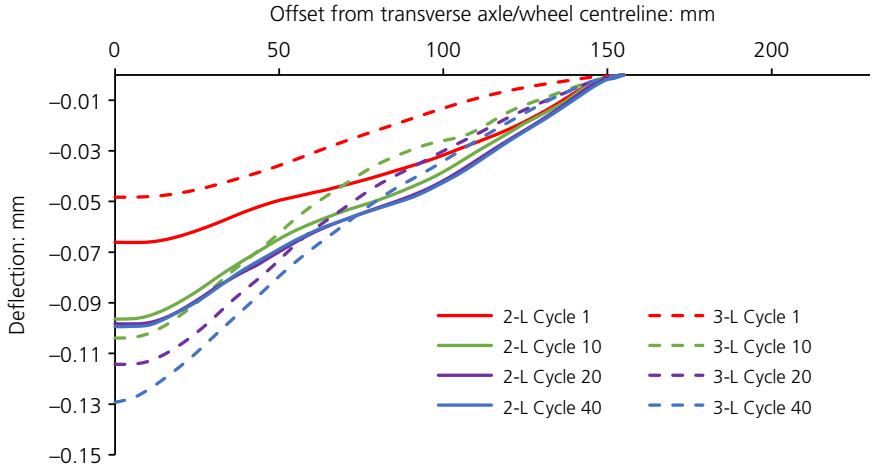

Figure 11. Deflection bowl change with cycle number

location when complex load configurations are used. The locations of critical parameters may not be where they are typically assumed to be if wheel interaction is considered.

- Incorporating cemented bases underneath an ultra-thin layer of HS-SFRC resulted in the overall displacement and permanent deformation being reduced. It was also observed that it may result in the base cracking discretely

and causing stress concentrations in the layers underneath it, which would in turn accelerate accumulation of permanent deformation.
- In the two-layer system, the concrete layer detached from the substructure when unloaded, indicating that a gap forms between concrete layer and the substructure. This loss of support could also result in the critical parameter locations moving to positions adjacent to the wheel path.

The results from this investigation indicate that the design assumptions made for neither rigid nor flexible pavements should be used when designing UTCRCP. The non-brittle, flexible nature of the HS-SFRC results in unique deflection bowls and stress distributions in the layers of the concrete pavement and unique design assumptions would be required to model the actual behaviour of UTCRCP.

Further research is also required to confirm both the possible deterioration of cement-stabilised layers used in UTCRCP and the detachment of the HS-SFRC layer from the substructure.

Acknowledgements

The authors thank the laboratory technicians, Johan Scholtz and Derek Mostert, at the University of Pretoria for the construction of the centrifuge pavement tester.

REFERENCES

ASTM (2006) D 4254: Standard test methods for minimum index density and unit weight of soils and calculation of relative density. ASTM International, West Conshohocken, PA, USA.

ASTM (2011) D 4253: Standard test methods for maximum index density and unit weight of soils using a vibratory table. ASTM International, West Conshohocken, PA, USA.

ASTM (2016a) D 4253-16: Standard test methods for maximum index density and unit weight of soils using vibratory table. ASTM International, West Conshohocken, PA, USA.

ASTM (2016b) D 4254-16: Standard test methods for minimum index density and unit weight of soils and calculation of relative density. ASTM International, West Conshohocken, PA, USA.

Barros JAO and Figueiras JA (1998) Experimental behavior of fiber concrete slabs on soil. *Mechanics of Cohesive-Frictional Materials* **3(3)**: 277–290.

Bayton SM, Elmrom T and Black JA (2018) Centrifuge modelling utility pipe behaviour subject to vehicular loading. In *Physical Modelling in Geotechnics (ICPMG 2018)* (McNamara A, Divall S, Goodey R *et al.* (eds)). Taylor & Francis Group, London, UK, pp. 163–168.

Belletti B, Cerioni R, Meda A and Plizzari G (2008) Design aspects on steel fiber-reinforced concrete pavements. *Journal of Materials in Civil Engineering* **20(9)**: 599–607.

Bowles JE (1996) *Foundation analysis and design*, 5th ed. New York, NY, USA: McGraw-Hill.

Briggs MA, Valsangkar AJ and Thompson A (2016) Behaviour of fibre-reinforced concrete beams on grade. *International Journal of Physical Modelling in Geotechnics* **16(4)**: 152–159, https://doi.org/10.1680/jphmg.15.00025.

Brown SF and Selig ET (1991) The design of pavement and rail track foundations. In *Cyclic Loading of Soils: From Theory to Design* (O'Reilly MP and Brown SF (eds)), 1st edn. Blackie, London, UK, pp. 249–305.

Gaspar TAV (2017) *The Tensile Behaviour of Three Unsaturated Soils Subjected to the Brazilian Disc Test*. Master's dissertation, University of Pretoria, Pretoria, South Africa.

Gerber JAK (2011) *Characterization of Crack on Ultra-Thin Continuously Reinforced Concrete Pavements*. Master's dissertation, Stellenbosch University, Stellenbosch, South Africa.

Huang YH (1993) *Pavement Analysis and Design*, 2nd edn. Prentice Hall, Upper Saddle River, NJ, USA.

Jacobsz SW, Kearsley EP and Kock JHL (2014) The geotechnical centrifuge facility at the University of Pretoria. In *Physical Modelling in Geotechnics (ICPMG 2014)* (Gaudin C and White D (eds)). CRC Press, Boca Raton, FL, USA, vol. 1, pp. 169–174.

Kannemeyer L, Perrie BD, Strauss PJ and Du Plessis L (2007) Ultra-thin continuously reinforced concrete pavement research in South Africa. In *Proceedings of the International Conference on Concrete Roads, 16–17 August 2007*. Cement & Concrete Institute, Midrand, South Africa, pp. 97–124.

Kearsley EP, Steyn WJVDM and Jacobsz SW (2014) Centrifuge modelling of ultra thin continuously reinforced concrete pavements (UTCRCP). In *Physical Modelling in Geotechnics (ICPMG 2014)* (Gaudin C and White D (eds)). CRC Press, Boca Raton, FL, USA, vol. 2, pp. 1101–1106.

Lukiantchuki J, Oliveira JRMS, Pessin J and Almeida M (2018) Centrifuge modelling of traffic simulation on a construction waste layer. *International Journal of Physical Modelling in Geotechnics* **18(6)**: 290–300, https://doi.org/10.1680/jphmg.17.00012.

Roesler JR, Cervantes VG and Amirkhanian AN (2012) Accelerated performance testing of concrete pavement with short slabs. *International Journal of Pavement Engineering* **13(6)**: 494–507.

Saboya F, Tibana S, Reis RM, Farfan AD and de Assis Melo CM (2020) Centrifuge and numerical modeling of moving traffic surface loads on pipeline buried in cohesionless soil. *Transportation Geotechnics* **23(2020)**: 1–11.

SANRAL (South African National Roads Agency Ltd) (2014) Road prism and pavement investigations. In *South African Pavement Engineering Manual*. SANRAL, Pretoria, South Africa, ch. 6.

Smit MS and Kearsley EP (2018) Investigating the response of ultra-thin continuously reinforced concrete pavements to initial loading. *Proceedings of the 13th International Symposium on Concrete Roads, 19–20 June 2018, Berlin, Germany.*

Smit MS, Kearsley EP and Jacobsz SW (2018) The effect of relative stiffness on soil-structure interaction under vehicle loads. In *Physical Modelling in Geotechnics (ICPMG 2018)* (McNamara A, Divall S, Goodey R *et al.* (eds)). Taylor & Francis Group, London, UK, pp. 185–190.

Strauss PJ, Slavik M, Kannemeyer L and Perrie BD (2007) Updating cncPave: inclusion of ultra-thin continuously reinforced concrete pavement (UTCRCP) in the mechanistic, empirical and risk based concrete pavement design method. In *Proceedings of the International Conference on Concrete*

Roads, 16–17 August 2007. Cement & Concrete Institute, Midrand, South Africa, pp. 204–218.

Westergaard HM (1926) Stresses in concrete pavements by theoretic analysis. *Public Roads* **7(2)**: 25–35.

Weyers M (2020) *Optimised Mix Composition and Structural Behaviour of Ultra-High-Performance Fibre Reinforced Concrete*. Master's dissertation, University of Pretoria, Pretoria, South Africa.